Structure of the He^4 Nucleus from Elastic Electron Scattering*

R. F. Frosch,† J. S. McCarthy, R. E. Rand,‡ and M. R. Yearian
High-Energy Physics Laboratory and Department of Physics, Stanford University, Stanford, California
(Received 7 April 1967)

We have measured the cross section for elastic electron scattering from He^4 at values of q^2, the four-momentum transfer squared, ranging from 0.5 to 20.0 F^{-2}. Previous Stanford measurements extended up to $q^2=6.2$ F^{-2} and were consistent with a Gaussian shape for the charge distribution of the He^4 nucleus. Our results confirm the earlier data but show a deviation from the Gaussian model for $q^2>6$ F^{-2}. At $q^2=10$ F^{-2} we observe a diffraction minimum of the scattering cross section. Among the models which have been found to fit the new data is the Fermi three-parameter charge distribution. The rms radius $\langle r^2\rangle^{1/2}$, the half-density radius $r_{1/2}$, and the 90% to 10% skin thickness t of the charge distribution have been calculated for the models which adequately fit the data. The results indicate that the surface of the He^4 charge distribution is less diffuse than implied by the nuclear harmonic-oscillator model.

I. INTRODUCTION

THE elastic scattering of high-energy electrons from He^4 has been studied some years ago by McAllister and Hofstadter,[1] Blankenbecler and Hofstadter,[2] Burleson and Kendall,[3] and Burleson.[4] These experiments provided values of the He^4 nuclear-charge form factor $F_{ch}(q^2)$ up to $q^2=6.2$ F^{-2} (where q^2 is the four-momentum transfer squared). In this range the experimental data are consistent with the Gaussian model

$$F_{ch}(q^2)=\exp[-\langle r^2\rangle q^2/6], \quad (1)$$

where $\langle r^2\rangle$ is the square of the rms radius of the nuclear charge distribution.[5] If very small effects due to nucleon structure are neglected, Eq. (1) agrees with the theoretical prediction based on the nuclear harmonic-oscillator potential.[5] The first indication of a deviation from the Gaussian form factor came from a recent experiment by Repellin *et al.*[6]; this experiment covered the range 2.5 $F^{-2}<q^2<8.1$ F^{-2}. The present series of measurements extending up to $q^2=20$ F^{-2} gives further evidence against the validity of the Gaussian model. A diffraction minimum of the form factor is observed at $q^2=10$ F^{-2}. This is the first time that a diffraction feature has been found in electron scattering from such a light nucleus.

II. APPARATUS

The previous electron scattering experiments on He^4 (Refs. 1–6) were performed with gaseous targets and, therefore, at large momentum transfers, suffered from low counting rates. In the present work a liquid-helium target was used. The electron beam was focused on a rectangular target cell of 12 mm thickness. This cell, which contained the liquid helium at atmosphere pressure, was formed from either 0.025 mm stainless steel or 0.025 mm aluminum alloy foils. An identical cell filled with liquid hydrogen was used for calibration purposes, and an empty cell was used for background measurements. The array of target cells and the cryogenic reservoirs are shown in Fig. 1. The liquid-helium target cell is filled with helium through an opening in the bottom of the 10 liter helium reservoir. This reservoir is surrounded by a liquid-hydrogen reservoir. For greater safety the hydrogen target is not connected directly to the H_2 reservoir, but instead gaseous H_2 in thermal contact with the reservoir is condensed into the target.[7] Two nitrogen tanks with attached thermal-radiation shields ensure that the central assembly is surrounded almost completely by surfaces at the temperature of liquid nitrogen. The nitrogen tanks and the radiation shields were covered with several insulated layers of aluminum foil in order to reduce the effects of thermal radiation. During the filling of the helium reservoir the liquid level was monitored by three electrical resistance indicators placed near the bottom, the center and the top of the reservoir. During the experiment the amount of liquid in the helium reservoir was determined by means of a gas flow meter placed in the helium vent line. The average helium vaporization rate was about 0.5 liters/h with the incident electron beam off and approximately 0.6 liters/h with the beam on ($\sim 6\times 10^{12}$ electrons/sec). Bubble formation in the helium target cell was investigated by measuring the same electron scattering cross section at various beam intensities. Bubbles were indeed detected at beam currents $\gtrsim 1$ μA if the amount of liquid remaining in the reservoir was less than 0.5 liters.

The Stanford mark III 1-GeV linear accelerator was used as the source of high-energy electrons. The electron

* Work supported in part by the U. S. Office of Naval Research, Contract No. Nonr 225(67).
† Present address: CERN, Geneva, Switzerland.
‡ Present address: Daresbury Nuclear Physics Laboratory, Daresbury, Lancashire, England.
[1] R. W. McAllister and R. Hofstadter, Phys. Rev. **102**, 851 (1956).
[2] R. Blankenbecler and R. Hofstadter, Bull. Am. Phys. Soc. **1**, 10 (1956).
[3] G. R. Burleson and H. W. Kendall, Nucl. Phys. **19**, 68 (1960).
[4] G. R. Burleson, Ph.D. thesis, Stanford University, 1960 (unpublished).
[5] R. Hofstadter, Rev. Mod. Phys. **28**, 214 (1956).
[6] J. P. Repellin, P. Lehmann, J. LeFrançois, and D. B. Isabelle, Phys. Letters **16**, 179 (1965).
[7] B. Chambers, R. Hofstadter, A. Marcum, and M. R. Yearian, in *Nucleon Structure, Proceedings of the International Conference at Stanford University, 1963* (Stanford University Press, Stanford, California, 1964), p. 361.

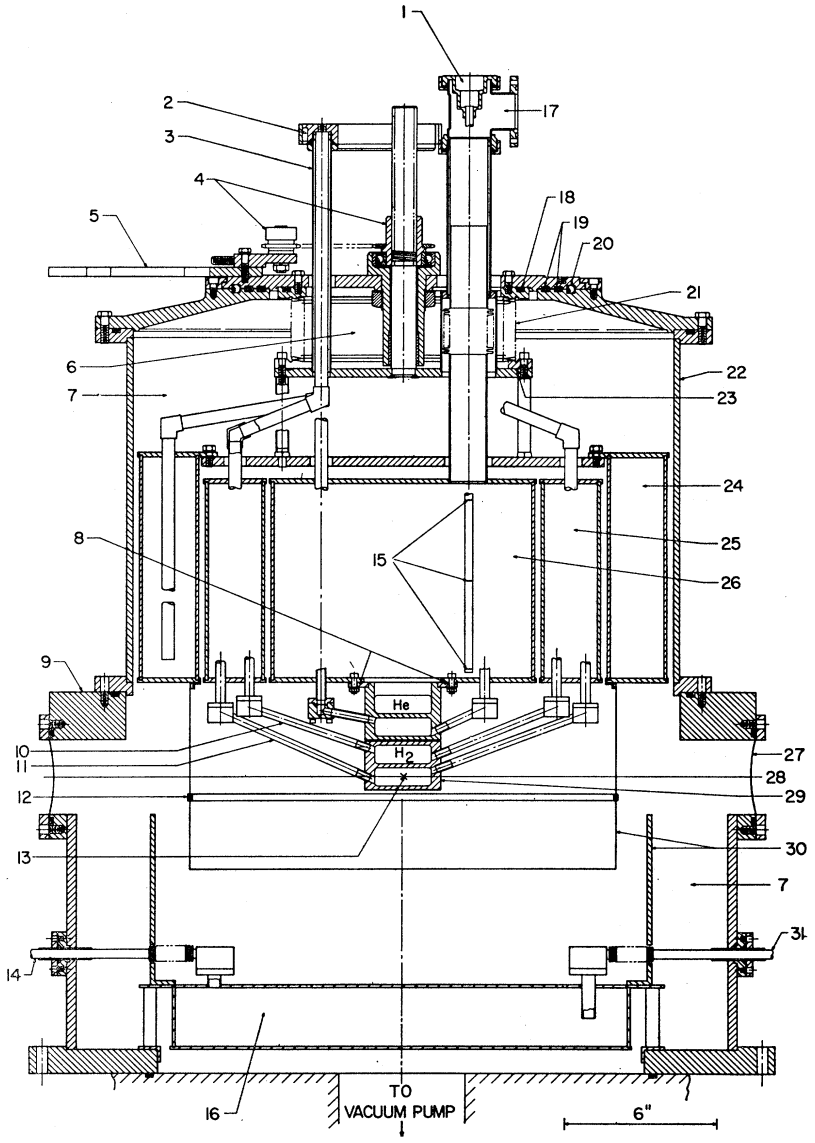

FIG. 1. Schematic drawing of the liquid-helium target (see text) in raised position.

1. 8-pole plug for level indicators.
2. Warming water.
3. Vacuum-jacketed port.
4. Target-lifting mechansim (chain driven).
5. Target-rotation lever.
6. Atmosphere.
7. Vacuum.
8. Indium seals.
9. Scattering chamber.
10. Target vent.
11. Target inlet.
12. Heat-shield frame.
13. Electron beam,
14. Nitrogen vent.
15. Liquid-helium level indicators.
16. Liquid-nitrogen reservoir (lower).
17. Helium vent.
18. O-ring seal.
19. Quad-ring seals.
20. Ball Bearing.
21. Bellows.
22. Upper vacuum chamber.
23. Lead seal.
24. Liquid-nitrogen reservoir (upper).
25. Liquid-hydrogen reservoir.
26. Liquid-helium reservoir.
27. Mylar window.
28. Beam level.
29. Target cells.
30. Heat shields.
31. Nitrogen inlet.

beam was monitored by a large Faraday cup placed behind the target. The scattered electrons were analyzed in momentum by a double-focusing spectrometer[8] and detected by an array of 100 scintillation counters, arranged in a ladder configuration, with Čerenkov backing counters (see Fig. 2).[9]

III. EXPERIMENTAL PROCEDURE

The accelerator was operated at incident electron energies E_0 ranging from 100 to 800 MeV, and the spectrometer was placed at scattering angles θ between 39° and 90°. A total of 45 cross sections at different values of E_0 and θ were measured. At the lower values of q^2, combinations of E_0 and θ were chosen such that groups of three or more cross sections having the same four-momentum transfer were obtained.

The spectra of electrons scattered from helium, hydrogen, and from an empty target were recorded. In the case of helium and hydrogen the spectrometer was set to transmit the elastic peak and a part of the associated radiative tail. The spectrometer settings for the background measurements were adjusted slightly to correct for the energy loss of the electrons due to ionization in the liquid. Two He^4 spectra corrected for background events are shown in Fig. 3. The momentum separation between elastically and inelastically scattered electrons is very large for He^4($\sim$20 MeV/c); therefore, it was

[8] R. Hofstadter, F. Bumiller, B. R. Chambers, and M. Croissiaux, in Proceedings of the International Conference on Instrumentation for High-Energy Physics, New York, 1961, p. 310 (unpublished).

[9] L. R. Suelzle and M. R. Yearian, in *Nucleon Structure, Proceedings of the International Conference at Stanford University, 1963* (Stanford University Press, Stanford, California, 1964), p. 360.

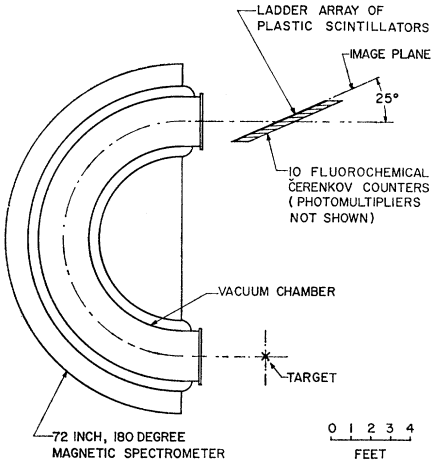

FIG. 2. Diagram of the spectrometer and the 100-channel detector.

not necessary to obtain high momentum resolution. In Fig. 3 the elastic peak and a small part of the broad peak due to the electrodisintegration of the α particle are shown.

The total area of the elastic peak including the radiative tail was calculated according to the theory of Tsai[10] using a computer program due to Crannell.[11] At cutoff momenta,[10] 10 MeV/c below the elastic peak, the radiative corrections ranged from 12 to 24%.

Absolute experimental cross sections for H_2 and He^4 were determined from the solid angle subtended by the spectrometer, the charge accumulated in the Faraday cup, and the target thickness. The target thickness

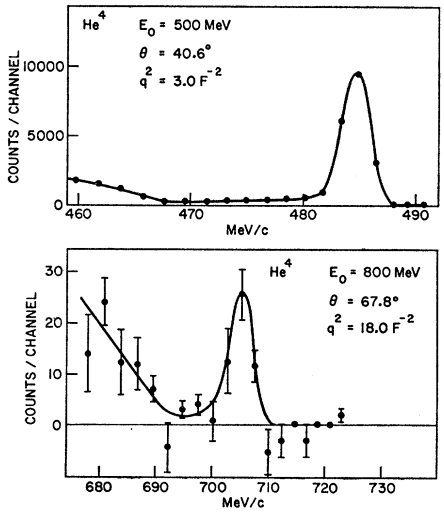

FIG. 3. Two spectra of electrons scattered from He^4, showing the elastic peak and part of the electrodisintegration spectrum. The solid curves drawn through the data points were not used in the analysis; the elastic-peak area was determined by summing the counts in all channels above the cutoff momentum (see Ref. 11).

[10] Y. S. Tsai, Phys. Rev. 120, 269 (1960).
[11] Hall Crannell, Phys. Rev. 148, 1107 (1966).

was measured optically using a travelling microscope. The densities of the liquid He and H_2 were obtained from the known vapor pressures. The relative efficiencies of the detectors were determined by measuring a smooth portion of the inelastic He^4 spectrum.[12] Assuming that the average absolute efficiency of the detectors was equal to unity, we obtained "uncorrected" cross sections $(d\sigma/d\Omega)_u$. The measured hydrogen cross sections $(d\sigma/d\Omega)_u^H$ were then compared with the values $(d\sigma/d\Omega)_c^H$ calculated from the proton form factors given by Janssens *et al.*[13] and the absolute efficiency ϵ

TABLE I. Experimental values of the cross section for elastic scattering of electrons from He^4. Here E is the incident electron energy, θ is the scattering angle, q^2 the four-momentum transfer squared, $d\sigma/d\Omega$ the experimental cross section, and F_{ch} the experimental charge form factor. In column 4, the number following the comma specifies the power of 10.

E (MeV)	θ (deg)	q^2 (F^{-2})	$d\sigma/d\Omega$ (cm^2/sr)	F_{ch}
100	90.0	0.50	(2.65 ±0.15), −30	0.796 ±0.024
103	90.0	0.53	(2.36 ±0.14), −30	0.788 ±0.024
150	56.0	0.50	(9.20 ±0.55), −30	0.796 ±0.024
	84.1	1.0	(9.80 ±0.59), −31	0.633 ±0.019
200	41.1	0.50	(1.845±0.11), −29	0.792 ±0.024
	60.0	1.0	(2.32 ±0.14), −30	0.619 ±0.019
	76.1	1.5	(5.18 ±0.31), −31	0.492 ±0.015
250	47.0	1.0	(4.23 ±0.25), −30	0.626 ±0.019
	58.8	1.5	(1.032±0.012), −30	0.496 ±0.015
	69.5	2.0	(3.10 ±0.19), −31	0.391 ±0.012
	89.8	3.0	(4.10 ±0.25), −32	0.256 ±0.008
300	48.2	1.5	(1.635±0.098), −30	0.493 ±0.015
	56.5	2.0	(5.27 ±0.32), −31	0.391 ±0.012
	86.0	4.0	(1.32 ±0.08), −32	0.1577±0.050
350	59.9	3.0	(1.25 ±0.08), −31	0.253 ±0.008
	81.9	5.0	(4.73 ±0.30), −33	0.0988±0.0030
400	41.4	2.0	(1.077±0.067), −30	0.390 ±0.012
	60.9	4.0	(3.53 ±0.22), −32	0.1600±0.0050
	78.0	6.0	(1.81 ±0.17), −33	0.0628±0.0030
500	40.6	3.0	(3.17 ±0.19), −31	0.255 ±0.008
	53.9	5.0	(1.41 ±0.09), −32	0.0976±0.0030
	59.9	6.0	(3.11 ±0.32), −33	0.0576±0.0030
	65.9	7.0	(6.97 ±0.96), −34	0.0335±0.0023
	71.3	8.0	(1.53 ±0.18), −34	0.0189±0.0011
601	39.1	4.0	(9.76 ±0.62), −32	0.1577+0.0050
	57.7	8.0	(2.58 ±0.49), −34	0.0182±0.0017
650	40.5	5.0	(2.51 ±0.16), −32	0.0932±0.0030
	48.8	7.0	(1.45 ±0.12), −33	0.0332±0.0014
	52.7	8.0	(1.95 ±0.64), −34	0.0143±0.0024
700	41.4	6.0	(7.70 ±0.80), −33	0.0582±0.0030
	48.5	8.0	(4.56 ±0.77), −34	0.0195±0.0018
800	39.0	7.0	(2.01 ±0.19), −33	0.0301±0.0014
	42.2	8.1	(4.87 ±0.59), −34	0.0175±0.0011
	43.4	8.5	(1.95 ±0.37), −34	0.0118±0.0011
	44.8	9.0	(5.79 ±2.55), −35	0.0069±0.0015
	46.2	9.5	(3.35 ±1.28), −35	0.0055±0.0011
	47.6	10.0	(9.2 ±7.9), −36	$0.0031_{-0.0019}{}^{+0.0002}$
	48.9	10.5	$(4.6_{-4.6}{}^{+5.9})$, −36	$0.0023_{-0.0023}{}^{+0.0019}$
	50.2	11.0	(1.43 ±0.49), −35	0.0043±0.0007
	52.9	12.0	(3.75 ±1.06), −35	0.0078±0.0011
	56.7	13.5	(3.96 ±0.66), −35	0.0094±0.0008
	60.4	15.0	(2.68 ±0.66), −35	0.0089±0.0011
	62.8	16.0	(2.76 ±0.43), −35	0.0098±0.0008
	67.8	18.0	(1.35 ±0.27), −35	0.0082±0.0008
	72.5	20.0	(7.2 ±1.9), −36	0.0070±0.0009

[12] Hall Crannell and L. R. Suelzle, Nucl. Instr. Methods 44, 133 (1966).
[13] T. Janssens, R. Hofstadter, E. B. Hughes, and M. R. Yearian, Phys. Rev. 142, 922 (1966).

was determined, where

$$\epsilon=\left(\frac{d\sigma}{d\Omega}\right)_u^{\mathrm{H}} \Big/ \left(\frac{d\sigma}{d\Omega}\right)_c^{\mathrm{H}}. \tag{2}$$

In Fig. 4, ϵ is plotted as a function of the scattered electron momentum for one of our runs. At large momenta, ϵ is consistent with unity, dropping below this value at the smallest momenta. This behavior results from the electrons with low momenta being stopped before reaching the backwall of the liquid Čerenkov counters[9] and therefore producing fewer photons than at higher momenta. The final result for the experimental He^4 cross section is

$$\left(\frac{d\sigma}{d\Omega}\right)^{\mathrm{He}^4}=\left(\frac{d\sigma}{d\Omega}\right)_u^{\mathrm{He}^4} \Big/ \epsilon(p), \tag{3}$$

where p is the momentum of the electrons elastically scattered from He^4.

IV. EXPERIMENTAL RESULTS

The experimental values of the cross sections for elastic electron scattering from He^4 are listed in Table I. The quoted errors of the cross sections have been obtained by quadratically adding the statistical uncertainty in the number of counted electrons in the elastic peak, and an estimate of the systematic error (typically ~6%) due to uncertainties in the target thickness and density, incident energy and scattering angle, radiative corrections, absolute efficiency, and of the charge integrated in the Faraday cup. The values of the charge form factor given in Table I were obtained

TABLE II. Experimental values of the He^4 charge form factor $F_{ch}(q^2)$.

q^2 (F^{-2})	$F_{ch}(q^2)$
0.5	0.796 ±0.025
1	0.626 ±0.030
1.5	0.494 ±0.015
2	0.391 ±0.012
3	0.225 ±0.008
4	0.1585±0.0050
5	0.0965±0.0030
6	0.0595±0.0030
7	0.0319±0.0014
8.0	0.0184±0.0011
8.1	0.0175±0.0011
8.5	0.0118±0.0011
9	0.0069±0.0015
9.5	0.0055±0.0011
10	$0.0031_{-0.0019}{}^{-0.0009}$
10.5	$0.0023_{-0.0023}{}^{+0.0012}$
11	0.0043±0.0007
12	0.0078±0.0011
13.5	0.0094±0.0008
15	0.0089±0.0011
16	0.0098±0.0008
18	0.0082±0.0008
20	0.0070±0.0009

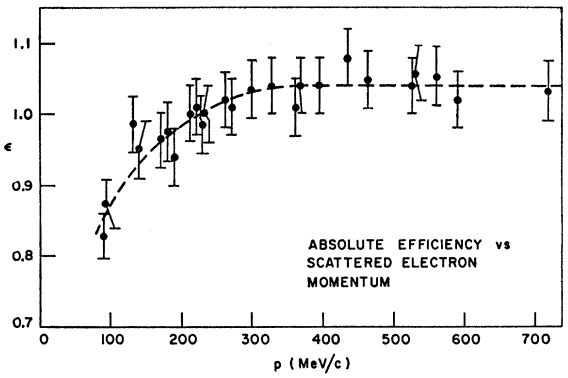

FIG. 4. Absolute efficiency of the counting system (see text). In the analysis we used the values defined by the dashed line which is a best fit through the data points.

using the formula[5]

$$F_{\mathrm{ch}}=\left[\left(\frac{d\sigma}{d\Omega}\right) \Big/ \left(\frac{d\sigma}{d\Omega}\right)_{\mathrm{point}}\right]^{1/2}, \tag{4}$$

where

$$\left(\frac{d\sigma}{d\Omega}\right)_{\mathrm{point}}=\left(\frac{Ze^2}{2E_0}\right)^2 \frac{\cos^2(\theta/2)}{\sin^4(\theta/2)} \frac{1}{1+(2E_0/Mc^2)\sin^2(\theta/2)} \tag{5}$$

is the cross section for elastic electron scattering from a spinless point particle with charge Ze and mass M. In the first Born approximation[5] the form factor F_{ch} as defined by Eq. (4) is a function of q^2 only, where

$$q^2=\left(\frac{2E_0}{ch}\right)^2 \frac{\sin^2(\theta/2)}{1+(2E_0/Mc^2)\sin^2(\theta/2)} \tag{6}$$

is the four-momentum transfer squared.

Our experimental values of $F_{\mathrm{ch}}(q^2)$ are presented in Table II and in Fig. 5. In the cases where more than one cross section was measured at the same q^2 value, a statistically weighted average was taken as the final

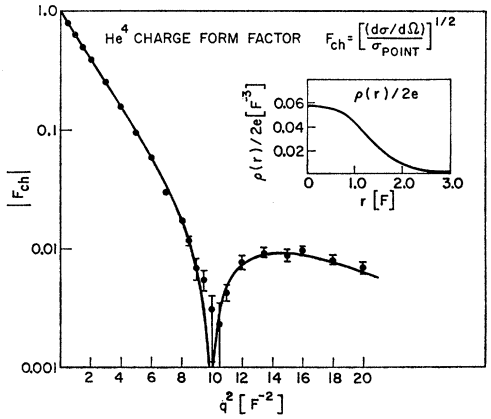

FIG. 5. Experimental values of the He^4 charge form factor (points) and values calculated from the charge distribution shown in the inset (solid curve).

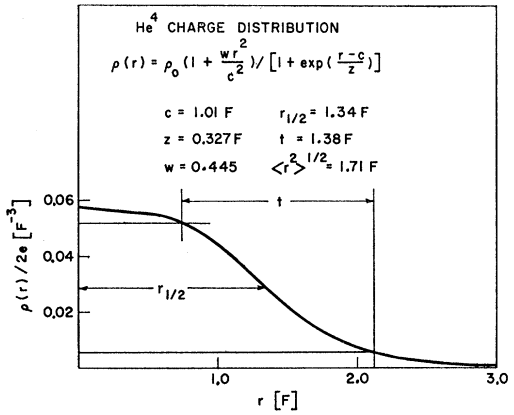

FIG. 6. He⁴ charge-density distribution obtained from a Born-approximation analysis using the Fermi three-parameter distribution function. The central depression, which usually occurs in this model, does not appear because of the comparatively large value of the ratio z/c.

result. In Fig. 5 only the results of this particular experiment are shown. A comparison of our data below $q^2=8$ F^{-2} with those of other authors has already been presented in an earlier publication.[14]

V. ANALYSIS

We have analyzed the new data assuming the validity of the first Born approximation. The accuracy of this approximation for electron scattering from light nuclei has been demonstrated elsewhere.[5,11,14] In the first Born approximation the charge form factor $F_{ch}(q^2)$ is the Fourier transform of the nuclear charge distribution $\rho(r)$:

$$F_{ch}(q^2)=4\pi\int_0^\infty \rho(r)j_0(qr)r^2\,dr. \tag{7}$$

The procedure commonly followed in the analysis of elastic electron scattering experiments is to try various analytical forms of $\rho(r)$, calculate $F_{ch}(q^2)$ according to Eq. (7), and compare the results with the experimental form-factor values. An alternative procedure[5] is to fit the experimental data with an analytical form of $F_{ch}(q^2)$ and then calculate the charge distribution from the inverted equation

$$\rho(r)=\frac{1}{2\pi^2}\int_0^\infty F_{ch}(q)j_0(qr)q^2\,dq \tag{8}$$

In both Eqs. (7) and (8) the total charge of the nucleus is assumed equal to unity.

In the present analysis we have obtained fits to the experimental data using both of the procdeures outlined above; i.e., we have searched for analytical models of the form factor $F_{ch}(q^2)$ and the charge distribution $\rho(r)$ which are consistent with the experimental results.

[14] R. F. Frosch, R. E. Rand, K. J. van Oostrum, and M. R. Yearian, Phys. Letters, 32, 598 (1966).

1. Analytical Form of the Charge Form Factor

A good fit to the new form-factor values was obtained using the expression

$$F_{ch}(q^2)=[1-(a^2q^2)^n]\exp(-b^2q^2), \tag{9}$$

with $n=6$; the best-fit values of the parameters a and b in Eq. (9) are

$$a=(0.316\pm0.001)\text{F},$$
$$b=(0.681\pm0.002)\text{F}.$$

The χ^2 value of the fit is 19.5 for 20 degrees of freedom. The errors assigned to a and b were obtained by changing these parameters until χ^2 had increased by unity. From the expression given in Eq. (9), the charge distribution $\rho(r)$ was calculated according to Eq. (8). The integral can be solved analytically; the resulting charge distribution is presented in the Appendix and also in Fig. 7. It should be noted that $\rho(r)$ determined by this method is slightly negative for large values of r; this is a reflection of the fact that the data are not available for $q^2>20$ F^{-2}. The rms radius $\langle r^2\rangle^{1/2}$, the half-density radius $r_{1/2}$, the 90 to 10% surface thickness t, and the central charge density $\rho(0)$ of this charge distribution are presented in Table III.

2. Analytical Forms of the Charge Distribution $\rho(r)$

The Gaussian charge distribution[5] does not lead to a diffraction minimum and is inconsistent with our data. The familiar Fermi and modified Gaussian charge distributions do not fit the data either. A good fit ($\chi^2=22$ for 19 degrees of freedom) could be obtained with the Fermi three-parameter distribution[5]

$$\rho(r)=\rho_0\left(1+\frac{wr^2}{c^2}\right)\Big/\left[1+\exp\left(\frac{r-c}{z}\right)\right]. \tag{10}$$

The best-fit parameters for Eq. (10) are

$$c=(1.008\pm0.013)\text{F},$$
$$z=(0.327\pm0.002)\text{F},$$
$$w=0.445\pm0.020.$$

TABLE III. Parameters of the He⁴ charge distribution. Here $\langle r^2\rangle^{1/2}$ is the root-mean-square radius of the charge distribution, $r_{1/2}$ is the half-density radius (see Fig. 6), and t is the 90% to 10% surface thickness (see Fig. 6).

Model	$\langle r^2\rangle^{1/2}$ (F)	$r_{1/2}$ (F)	t (F)	$\rho(0)$ (F^{-3})
Fermi three-parameter, Eq. (10)	1.71	1.34	1.38	0.0577[c]
Fourier transform of Eq. (9)	1.67	1.32	1.45	0.0595[c]
Gaussian[a]	1.68	1.14	1.64	0.0698[c]
Gaussian[b]	1.63±0.04	···	···	···

[a] Reference 5.
[b] Reference 15.
[c] The central charge density $\rho(0)$ was calculated assuming the total charge of the nucleus equal to unity.

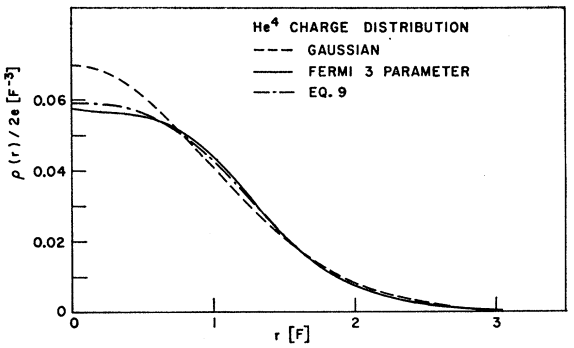

FIG. 7. Three models for the He^4 nuclear charge distribution. The Gaussian model fits the data only up to $q^2 \approx 6$ F^{-2}, whereas the Fermi three-parameter distribution and the model given by Eq. (9) [see also Eq. (A2)] fit all the data.

This charge distribution is shown in Figs. 6 and 7 and also in the inset of Fig. 5. The rms radius, the half-density radius, the 90 to 10% skin thickness and the central charge density are given in Table III. For comparison, the parameters for the Gaussian charge distribution fitted to the points at $q^2 \leqq 6$ F^{-2} are also shown in Table III, along with the rms value determined in a recent low-q^2 experiment by Frank, Haas, and Prange[15] at Darmstadt. As the rms radius can be determined in a model-independent way from the slope of the form-factor curve at $q^2=0$, the rms radius obtained from the low-q^2 experiment[15] is at present the most reliable estimate. As to the remaining parameters, the values given in Table III indicate that the surface of the He^4 charge distribution is less diffuse than previously implied by the Gaussian model fitted to the earlier data. This conclusion is also evident from Fig. 7, where the charge distributions given in the first three lines of Table III are plotted.

VI. CONCLUSIONS

By measuring the absolute cross sections for elastic electron scattering from He^4 over a large range in four-momentum transfers, we have found conclusive evidence for a deviation from the Gaussian model of the He^4 nucleus. The surface of the true charge distribution appears to be less diffuse than indicated by the Gaussian model. The observed deviations from the Gaussian model imply that in the shell-model description of the nucleus, the harmonic-oscillator potential is inadequate for He^4.

ACKNOWLEDGMENTS

We thank Professor R. Hofstadter for his continuing support of this work, as well as the staff of the high-energy physics laboratory without whose efforts the experiment would not have been possible. We further acknowledge the assistance of R. S. Safrata who gave advice on cryogenic problems, and we thank C. Littig for his help in taking the data. Our most cordial thanks are also due to L. Suelzle and H. Crannell for their assistance in the operation of the 100-channel ladder detector and the related data analysis. The successful operation of the liquid-helium target was made possible by the help of A. I. Marcum, G. Pryke, M. Ryneveld, and G. Lane.

APPENDIX

In order to obtain the charge distribution $\rho(r)$ from the charge form factor defined in Eq. (9), the following integral must be solved:

$$\rho(r)=\frac{1}{2\pi^2}\int_0^\infty [1-(a^2q^2)^n][\exp(-b^2q^2)]j_0(qr)dq. \quad \text{(A1)}$$

This integral can be solved analytically with the help of standard tables, e.g., Ref. 16. For $n=6$, the result is

$$\rho(r)=\rho(0)\left\{1+\frac{(2a)^{12}}{c}\left[\frac{135135}{16}\left(\frac{r}{2b}\right)^2-\frac{135135}{16}\left(\frac{r}{2b}\right)^4+\frac{6435}{2}\left(\frac{r}{2b}\right)^6-\frac{2145}{4}\left(\frac{r}{2b}\right)^8+39\left(\frac{r}{2b}\right)^{10}-\left(\frac{r}{2b}\right)^{12}\right]\right\}\exp(-r^2/4b^2),$$

where

$$c=(2b)^{12}-[(13)!!]\times 2^{-6}(2a)^{12},$$

and

$$\rho(0)=c/[\pi^{3/2}(2b)^{15}]. \quad \text{(A2)}$$

[15] H. Frank, D. Haas, and H. Prange, Phys. Letters **19**, 391 (1965); **19**, 719 (1965).

[16] D. Bierens de Haan, *Nouvelles Tables d'Intégrales Définies* (G. E. Stechert and Company, New York, 1939), p. 506.